Simulation and Analysis of Modon Motion in an Inviscid and Confined Fluid Environment

George Tang

Supervisor: Matthew N. Crowe

May 2023

1 Introduction

The objective of this paper is to explore the nature of dipole vortices and investigate their interaction dynamics. The analysis begins in Section 2, where we derive the quasigeostrophic equation by starting with the basic rotating shallow water equations. This equation proves to be invaluable for the examination of dipole vortices. In Section 3, we employ the implicit function theorem to derive a vorticity equation. Drawing inspiration from the influential work of Meleshko and van Heijst (1994), we introduce a linear relationship for the derived vorticity equation. Furthermore, we present distinct equations for both the stationary frame and the relative moving frame. These equations serve a vital purpose in establishing the initial conditions necessary for the subsequent Python simulation. By considering both frames, we gain a comprehensive understanding of the dynamics and behaviors of the dipole vortices within different reference frames.

In Section 4, a concise introduction outlines the formation of dipole vortices. I then delve into a detailed explanation of the solutions to the quasigeostrophic equation described in Sections 2 and 3. To aid comprehension, visual illustrations in the form of Python plots are presented, providing a visual understanding of the dipole vortex shapes.

I utilized the Dedalus package in Python to conduct simulations of dipole vortices, which serves as the focal point of our analysis. Section 5 delves into the implementation details, providing comprehensive explanations of the underlying mathematics at play. i.e. To address errors arising from numerical analysis, additional terms were introduced into the system, which were not originally part of our problem. One such concept is Numerical viscosity, which I introduced to account for the impact of the Gibbs phenomenon that arises due to the use of a finite grid model with Fourier approximation functions. Consequently, the dipole vortices fail to converge when they intersect the boundary. Subsequently in this section, I examine various types of motion exhibited by the dipole vortices, considering different scattering effects.

In section 6, I propose treating the dipole vortices as a point vortex model. Within this chapter, I employ Python to generate plots illustrating the trajectories of the point vortices. Remarkably, I discover that their paths coincide with the simulations presented in section 5.

2 Quasigeostrophic equation

[3] Firstly we introduced the Coriolis coefficient

$$f = 2\Omega \sin \lambda$$

where $\Omega \sin \lambda \vec{z}$ is perpendicular to $\vec{u}$ on the spherical earth locally. Take D to be the average depth with $h_B(x, y)$ to be the base of our model. Then we can define the undisturbed depth to be $D - h_B = H_0(x, y)$ and the instantaneous depth to be $H(x, y, t) = H_0(x, y) + \eta(x, y, t)$. Now consider the rotating shallow water equations(rSWE):

$$\begin{cases} \frac{Du}{Dt} - fv = -g\frac{\partial \eta}{\partial x} \\ \frac{Dv}{Dt} + fu = -g\frac{\partial \eta}{\partial y} \\ \frac{DH}{Dt} + H\nabla \cdot \vec{u} = 0 \end{cases} \tag{1}$$

Now I would like to introduce the non-dimensional quantity(normalizing or eliminating the dimensions of a physical quantity) :

$$\begin{cases} (x,y) = L(x',y') \\ t = Tt' \\ (u,v) = U(u',v') \\ \eta = N_0\eta' \end{cases} \tag{2}$$

Our rSWE will become:

$$\begin{cases} \frac{U}{T}\frac{\partial u'}{\partial t'} + \frac{U^2}{L}(u'\frac{\partial u'}{\partial x'} + v'\frac{\partial u'}{\partial y'}) - Ufv' = -\frac{gN_0}{L}\frac{\partial \eta'}{\partial x'} \\ \frac{U}{T}\frac{\partial v'}{\partial t'} + \frac{U^2}{L}(u'\frac{\partial v'}{\partial x'} + v'\frac{\partial v'}{\partial y'}) + Ufu' = -\frac{gN_0}{L}\frac{\partial \eta'}{\partial y'} \\ \frac{N_0}{T}\frac{\partial \eta'}{\partial t'} + \frac{U}{L}[u'\frac{\partial}{\partial x'}(N_0\eta' - h_B) + v'\frac{\partial}{\partial y'}(N_0\eta' - h_B)] + \frac{U}{L}(D + N_0\eta' - h_B)(\frac{\partial u'}{\partial x'} + \frac{\partial v'}{\partial y'}) = 0 \end{cases} \tag{3}$$

- Since we know pressure gradient need to equal to the Coriolis force as our leading order term need to be geostrophic balance,

$$N_0\frac{g}{L} = Uf$$

- The ratio of the nonlinear term to the Coriolis term is

$$\frac{U^2/L}{Uf} = \frac{U}{fL} = \epsilon$$

  This is the Rossby number.

- The ratio of the time dependent term to the Coriolis term is

$$\frac{U/T}{Uf} = \frac{1}{fT} = \epsilon_T$$

  , which we call it the temporal Rossby number.

- Cconsider $\frac{N_0}{D} = \frac{UfL}{gD}$. We know gD is the speed of the longest wave so $gD = c^2$. Therefore $\frac{N_0}{D} = \frac{U}{fL}(\frac{L}{a})^2 = \epsilon(\frac{L}{a})^2 = \epsilon F$ where $a = \frac{c}{f}$ is the Rossby radius.

We can divide the first two equation of 3 by Uf and our continuity equation by $\frac{UD}{L}$ and drop off the primes:

$$\begin{cases} \epsilon_T\frac{\partial u}{\partial t} + \epsilon(u\frac{\partial u}{\partial x} + v\frac{\partial u}{\partial y}) - v = -\frac{\partial \eta}{\partial x} \\ \epsilon_T\frac{\partial v}{\partial t} + \epsilon(u\frac{\partial v}{\partial x} + v\frac{\partial v}{\partial y}) + u = -\frac{\partial \eta}{\partial y} \\ \epsilon_T F\frac{\partial \eta}{\partial t} + \epsilon F(u\frac{\partial \eta}{\partial x} + v\frac{\partial \eta}{\partial y}) - u\frac{\partial}{\partial x}(\frac{h_B}{D}) - v\frac{\partial}{\partial y}(\frac{h_B}{D}) + (1 + \epsilon F\eta - \frac{h_B}{D})(\frac{\partial u}{\partial x} + \frac{\partial v}{\partial y}) = 0 \end{cases} \tag{4}$$

We want to find the behaviour of the system when ϵ, ϵ_T are both small, however, since there are two variables we need to look at its limits sperately. Now we only consider the case when $1 >> \epsilon \sim \epsilon_T$. This is the case when we have the time dependence and nonlinearity in our equation with no poincare waves.

$$\begin{cases} \epsilon(\frac{\partial u}{\partial t} + u\frac{\partial u}{\partial x} + v\frac{\partial u}{\partial y}) - v = -\frac{\partial \eta}{\partial x} \\ \epsilon(\frac{\partial v}{\partial t} + u\frac{\partial v}{\partial x} + v\frac{\partial v}{\partial y}) + u = -\frac{\partial \eta}{\partial y} \\ \epsilon F(\frac{\partial \eta}{\partial t} + u\frac{\partial \eta}{\partial x} + v\frac{\partial \eta}{\partial y}) - u\frac{\partial}{\partial x}(\frac{h_B}{D}) - v\frac{\partial}{\partial y}(\frac{h_B}{D}) + (1 + \epsilon F\eta - \frac{h_B}{D})(\frac{\partial u}{\partial x} + \frac{\partial v}{\partial y}) = 0 \end{cases} \tag{5}$$

Consider a taylor expansion of u in ϵ:

$$u(x,y,t;\epsilon) = u^{(0)} + \epsilon u^{(1)} + \epsilon^2 u^{(2)} + \cdots$$

Consider the $\epsilon^{(0)}$ term: The momentum equation will give us the following:

$$\begin{cases} -v^{(0)} = -\frac{\partial \eta^{(0)}}{\partial x} \\ u^{(0)} = -\frac{\partial \eta^{(0)}}{\partial y} \end{cases} \tag{6}$$

This shows η is our streamfunction which means it satisfied the impressible condition: $\nabla \cdot \vec{u} = 0$. We can deduce from the continuity equation that

$$-u^{(0)}\frac{\partial}{\partial x}(\frac{h_B}{D}) - v^{(0)}\frac{\partial}{\partial y}(\frac{h_B}{D}) = 0$$

with the assumption $h_B/D \sim 1$ However, in open oceans this is usually not true. we usually have $h_B/D \sim \epsilon$ i.e.

$$\frac{h_B}{D} = \epsilon\eta_B(x,y)$$

Then we look at the order ϵ terms of the continuity equation and find:

$$F\frac{D\eta^{(0)}}{Dt} - u^{(0)}\frac{\partial\eta_B}{\partial x} - v^{(0)}\frac{\partial\eta_B}{\partial y} + \frac{\partial u^{(1)}}{\partial x} + \frac{\partial v^{(1)}}{\partial y} = 0 \tag{7}$$

We now go to the order ϵ term of the momentum equations:

$$\begin{cases} \frac{Du^{(0)}}{Dt} - v^{(1)} = -\frac{\partial\eta^{(1)}}{\partial x} \\ \frac{Dv^{(0)}}{Dt} + u^{(1)} = -\frac{\partial\eta^{(1)}}{\partial y} \end{cases} \tag{8}$$

To get rid of $\eta^{(1)}$, we can do the following to (8):

$$\begin{cases} \frac{D}{Dt}(\frac{\partial u^{(0)}}{\partial y}) - \frac{\partial v^{(1)}}{\partial y} = -\frac{\partial^2\eta^{(1)}}{\partial x\partial y} \\ \frac{D}{Dt}(\frac{\partial v^{(0)}}{\partial x}) + \frac{\partial u^{(1)}}{\partial x} = -\frac{\partial^2\eta^{(1)}}{\partial y\partial x} \end{cases} \tag{9}$$

Then by take the difference of them, we obtain:

$$\frac{D\zeta^{(0)}}{Dt} + \frac{\partial u^{(1)}}{\partial x} + \frac{\partial v^{(1)}}{\partial y} = 0 \tag{10}$$

where $\zeta = \frac{\partial v^{(0)}}{\partial x} - \frac{\partial u^{(0)}}{\partial y}$. Now taking the difference between (7) and (10) we get:

$$\frac{Dq^{(0)}}{Dt} = 0 \tag{11}$$

where $q^{(0)} = \zeta^{(0)} - F\eta^{(0)} + \eta_B$ We can show this is the **conservation of quasigeostrophic potential vorticity**. We know the dimensional potential vorticity is defined as

$$q^* = \frac{\zeta^* + f}{H^*} \tag{12}$$

$$= \frac{f}{D}\frac{\epsilon\zeta + 1}{1 + \epsilon F\eta - \epsilon\eta_B} \qquad H = D(1 + \epsilon F\eta' - \frac{h_B}{D}) \tag{13}$$

$$= \frac{f}{D}(1 + \epsilon\zeta)(1 - \epsilon F\eta + \epsilon\zeta_B) \tag{14}$$

$$= \frac{f}{D}(1 + \epsilon(\zeta - F\eta + \eta_B)) \tag{15}$$

If we ignore 1, then it is clear that q is the nondimensional potential vorticity.
Since η acts as a stream function, we can rewrite it as the following:

$$(\frac{\partial}{\partial t} + \frac{\partial\psi}{\partial x}\frac{\partial}{\partial y} - \frac{\partial\psi}{\partial y}\frac{\partial}{\partial x})(\nabla^2\psi - F\psi + \eta_B) = 0 \tag{16}$$

and let's denote $\Pi = \nabla^2\psi - F\psi + \eta_B$. From now on, I am going to assume the height of the bottom has constant height. Therefore, $\frac{h_B}{D}$ is just constant and we could ignore,

$$(\frac{\partial\psi}{\partial x}\frac{\partial}{\partial y} - \frac{\partial\psi}{\partial y}\frac{\partial}{\partial x})(\nabla^2\psi - F\psi) = 0 \tag{17}$$

3 Steady quasigeotrophic motion

If the motion is independent of time, the quasigeostrophic potential-vorticity equation reduces to $J[\psi, \Pi] = 0$. I claim if the jacobian of two function is 0 then one function must be in term of the other(This is known as the implicit function theorem:

Proof. Firstly consider Jacobian of two arbitrary function is $J[f,g]$ and set $J[f,g] = 0$. Then we can rewrite this as

$$J[f,g] = \begin{pmatrix} \frac{\partial f}{\partial x} \\ \frac{\partial f}{\partial y} \end{pmatrix} \cdot \begin{pmatrix} \frac{\partial g}{\partial y} \\ -\frac{\partial g}{\partial x} \end{pmatrix} = 0$$

This means those two vector are orthogonal to each other. Hence $\nabla f \parallel \nabla g$ implies the level surface of f and g are parallel to each other. This means for each level surface, g need to take the same value as f does. Therefore, we can find a function q which map f to g. i.e. $g(x,y) = q(f(x,y))$ □

Therefore $\Pi = G(\psi) \implies \nabla^2\psi - F\psi = G(\psi) \implies \nabla^2\psi = K(\psi)$ where K is a function in terms of ψ.

Suppose the system is not independent of time, in fact, it is travelling at a speed c along the x direction. Then we can use the method of coordinate transformation:

$$\begin{cases} x' = x - ct \\ t' = t \\ y' = y \end{cases} \tag{18}$$

Then, by chain rule, we have:

$$\begin{cases} \frac{\partial}{\partial t} = \frac{\partial}{\partial t'} - c\frac{\partial}{\partial x'} \\ \frac{\partial}{\partial x} = \frac{\partial}{\partial x'} \\ \frac{\partial}{\partial y} = \frac{\partial}{\partial y'} \end{cases} \tag{19}$$

Since using this change of coordinate, we are moving along the system with speed c. Therefore, in our prospective view, the system is stationary: $\frac{\partial}{\partial t} = -c\frac{\partial}{\partial x'}$. Then (16) can be written as

$$-c\frac{\partial \Pi}{\partial x'} + J[\psi, \Pi] = 0$$

Since c is a constant, it can be written as $\frac{\partial}{\partial y}cy$, and our problem become:

$$-\frac{\partial}{\partial y}cy\frac{\partial \Pi}{\partial x'} + J[\psi, \Pi] = 0 \tag{20}$$

$$J[\psi + cy, \Pi] = 0 \tag{21}$$

Then by implicit function theorem, we know $\Pi = G(\psi + cy)$ where G is a function in terms of $\psi + cy$. Same argument as before, we will have $\nabla^2\psi = F\psi + G(\psi + cy)$

4 Dipole vortices moving along a straight line

4.1 Symmetrical dipole in an unbounded fluid

Before I dive into the formula of dipole vortices, I would like to point out how it is formed. 'Dipole formation and collisions in a stratified fluid' [8] by G. J. F. van Heijst & J. B. Flor demostrated the formation of two-dimensional dipole structures by the gravitational collapse of a compact region of three dimensionally turbulent, mixed fluid in a quiescent stratified environment. In their paper, he has briefly described the set up: 'It was conducted in a square perspex tank of horizontal dimensions 1 x 1 m and a working depth of 0.3 m, which was filled with a linearly stratified salt solution. A fixed volume of fluid was injected horizontally through a nozzle with a small diameter d. The injection velocity U was typically $2ms^{-1}$, the nozzle diameter $d \approx 10^{-3}m$ and the kinematic fluid viscosity $v \approx 10^{-6}m^2s^{-1}$, so that the Reynolds number, based on the nozzle diameter, had a characteristic value greater than $2x10^3$, which ensured that the outflow was turbulent.' The formation of dipole vortex was recorded by cameras as shown in Figure(1)

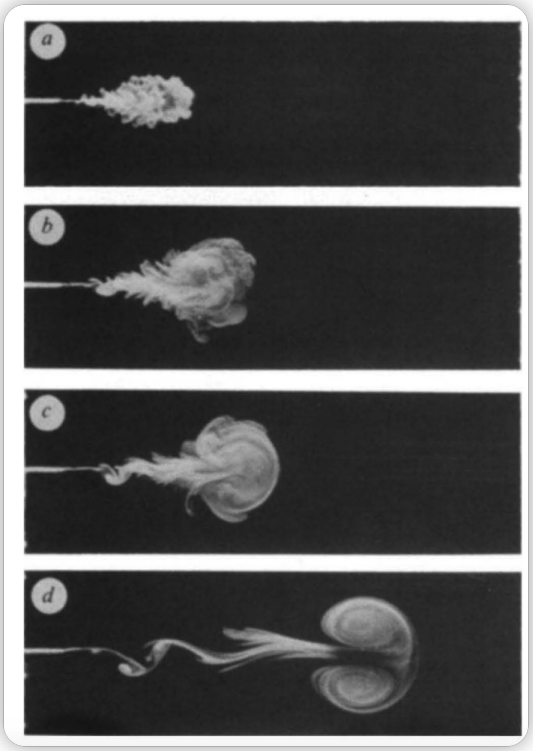

Figure 1: formation of dipole vortex

The question now is how can we present this dipole vortex mathematically. In 1903 Chaplygin published a paper which introduced the idea of a dipolar vortices moving along a straight line. He gave a precise formulation of the problem: [4]
'Consider an unbounded mass of incompressible fluid in which the motion is parallel to the OXY plane; let the motion outside some circular cylinder be irrotational, the velocity being equal to zero at infinity. The question is to find a distribution of vortices lines inside the cylinder that gives rise to a uniformly translating vortices column with a continuous velocity distribution and with a positive pressure all around.'

Using the idea described in 'page 166, Meleshko van Heijst 1994'. We can treat this problem as rectilinear motion of a circular vortices of radius a with a constant translation velocity U. We can superimposing on the whole fluid a uniform velocity -U, and obtained a stationary problem of a steady vortices cylinder placed in a potential flow. In this prospective, we have obtain a problem where the far field fluid is moving and the vortices is stationary. (Instead of solving (21), we can solve $\nabla^2\psi = K(\psi)$)

We have the governing equation $\nabla^2\psi = K(\psi)$. The first person to solve this problem was Lamb, and in his second edition of his treatise Hydrodynamics(1895), he consider the linear solution to this problem: $K(\psi) = -k^2\psi$. I verified his result and obtain the following: Consider the equation in (r, θ) coordinate and consider the separation solution $\psi = F(r)G(\theta)$. We will obtain the following:

$$\frac{F_{rr} + \frac{1}{r}F_r + kF}{\frac{F}{r^2}} = -\frac{G_{\theta\theta}}{G} \tag{22}$$

Since we have $\psi = 0$ at $r = a$, we can treat the LHS as a sturm-liouville problem. We can use the substitution $z = \sqrt{k}r, H(z) = F(r)$, then the LHS become:

$$H_{zz} + \frac{H_z}{z} + (1 - \frac{n^2}{z^2})H = 0 \tag{23}$$

which is a standard Bessel equation with index n. It has the solution $H = J_n(z)$. Therefore $F(r) = J_n(\sqrt{k}r)$
After substitute in the boundary condition and solve the RHS we will obtain:

$$\psi = \sum_{n=1}^{\infty} C_n J_n(\frac{j_{ni}r}{a}) \sin n\theta \tag{24}$$

where j_{ni} are known as the Bessel zeros. Outside the circle we have $\psi_1 = U(r - \frac{a^2}{r}) \sin\theta$

1. In order for both ψ and ψ_1 agree for $r = a$ (since velocity distribution is continuous), we need $n = 1$

2. We also need $\frac{\partial \psi}{\partial r} = \frac{\partial \psi_1}{\partial r}$ at $r = a$.

$$U(1 + \frac{a^2}{r^2}) \sin\theta = \frac{j_{1i}}{a} C J_1'(\frac{j_{1i} r}{a}) \sin\theta \tag{25}$$

$$2U = \frac{j_{1i}}{a} C J_0(j_{1i}) \qquad J_0(x) = J_1'(x) \tag{26}$$

$$C = \frac{2Ua}{j_{1i} J_0(j_{1i})} \tag{27}$$

Therefore we have our final steady solution:

$$\begin{cases} \psi(r,\theta) = \frac{2Ua}{j_{1i} J_0(j_{1i})} J_1(\frac{j_{1i} r}{a}) \sin\theta, & r \le a \\ \psi_1 = U(r - \frac{a^2}{r}) \sin\theta, & r > a \end{cases} \tag{28}$$

However, you will see later, when we do the simulation, we need the vortices moving instead. Therefore, we have our governing equation:

$$\begin{cases} \hat{\psi}(r,\theta) = (-Ur + \frac{2Ua}{j_{1i} J_0(j_{1i})} J_1(\frac{j_{1i} r}{a})) \sin\theta, & r \le a \\ \hat{\psi}_1 = -U\frac{a^2}{r} \sin\theta, & r > a \end{cases} \tag{29}$$

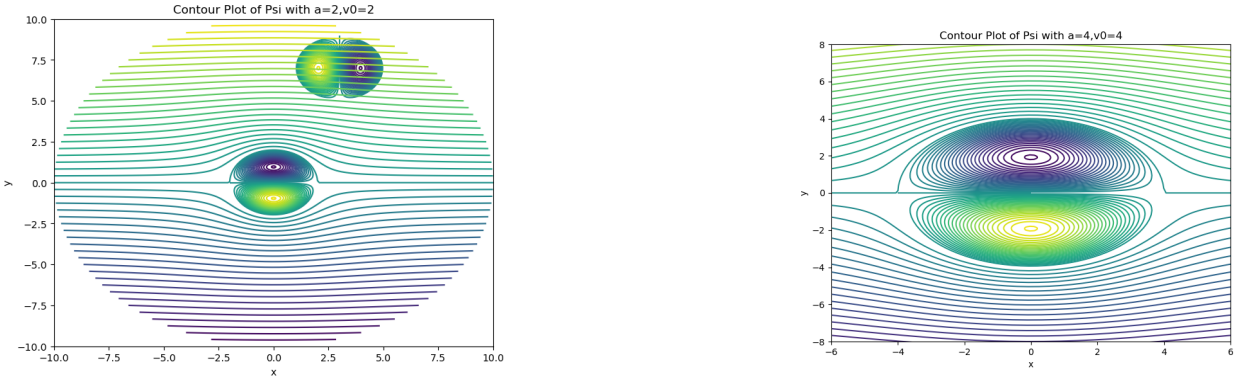

(a) Symmetric dipole vortices 1

(b) Symmetric dipole vortices 2

Figure 2: Symmetric dipole vortices

4.2 Non-symmetric dipole vortices

By taking $K(\psi) = -n^2(\psi - \lambda)$ where n, λ are constant. Then we obtain a solution with the interior vortices flow being asymmetric with respect to the OX-axis.

$$\psi(r,\theta) = \frac{2Ua}{j_{1i} J_0(j_{1i})} J_1(\frac{j_{1i} r}{a}) \sin n\theta + \lambda(1 - \frac{J_0(\frac{j_{1i} r}{a})}{J_0(j_{1i})}), \quad r \le a \tag{30}$$

As suggested in figure (3a),(3b), the ratio $\frac{\lambda}{av_0}$ determine the flow. With increasing values of λ the structure of the streamline gradually changes into that of a monopolar vortices.

5 Simulation

5.1 Setting Up the Problem

I used **Daedalus** package for the following simulation. The purposes Dedalus is to provide a framework applying modern sparse sepectral techiques to highly parallelized simulations of custom PDES. [9] For more information, please visit here. The following is the code for the simulation.

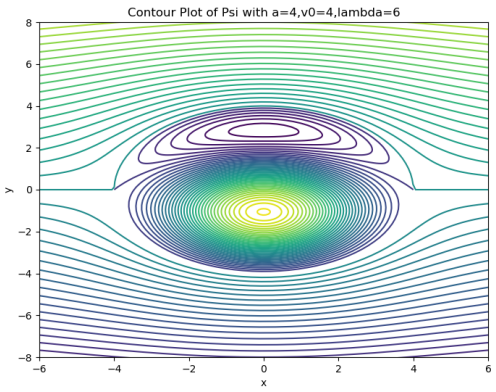

(a) Non-symmetric dipole vortices 1

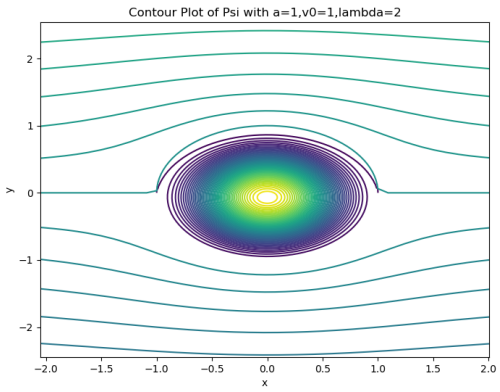

(b) Non-symmetric dipole vortices 2

Figure 3: Non-symmetric dipole vortices

```
"""
    $ mpiexec -n 4 python3 shear_flow.py
    $ mpiexec -n 4 python3 plot_snapshots.py snapshots/*.h5
"""

import numpy as np
import dedalus.public as d3
import logging
from scipy.special import jvp,j1
logger = logging.getLogger(__name__)


# Parameters
Lx, Ly = 20, 20
Nx, Ny = 256, 256
stop_sim_time = 10
max_timestep = 0.5e-3 #when I tried to use 1e2, the jump since effect the energy equation
nu = 0.1*(2*Lx/Nx)**2


dealias = 3/2
timestepper = d3.RK222
dtype = np.float64

# Bases
coords = d3.CartesianCoordinates('x', 'y')
dist = d3.Distributor(coords, dtype=dtype)
xbasis = d3.RealFourier(coords['x'], size=Nx, bounds=(-Lx/2, Lx), dealias=dealias)
ybasis = d3.RealFourier(coords['y'], size=Ny, bounds=(-Ly, Ly), dealias=dealias)

# Fields
psi = dist.Field(name='psi', bases=(xbasis,ybasis))
tau = dist.Field(name='tau')
# Substitutions
x, y = dist.local_grids(xbasis, ybasis)
dx = lambda A: d3.Differentiate(A,coords[0])
dy = lambda A: d3.Differentiate(A,coords[1])
J = lambda A,B: dx(A)*dy(B)-dx(B)*dy(A)
b=3.8317
# Problem
problem = d3.IVP([psi, tau], namespace=locals()) #One single boundry condition, so one single tau term required
problem.add_equation("dt(lap(psi)) + tau - nu*lap(lap(psi)) = - J(psi,lap(psi))")
problem.add_equation("integ(psi) = 0")
```

```
44
45  # Solver
46  solver = problem.build_solver(timestepper)
47  solver.stop_sim_time = stop_sim_time
48
49
50  # define lap(psi)
51  def vortex_vorticity(a,U,x0,y0,theta):
52      b = 3.83171
53      r = np.sqrt((x-x0)**2+(y-y0)**2)
54      t = np.arctan2(y-y0,x-x0)-theta
55      return -b*U*2*j1(b*r/a)/(a*jvp(1,b))*np.heaviside(a-r,1)*np.sin(t)
56
57  # we calculate lap(psi) using lap(psi) = -b^2*(psi+Uy) inside the vortex and lap(psi) = 0 outside, (this is in the lab frame)
58  vor0 = dist.Field(name='vor0', bases=(xbasis,ybasis))    # new field, will be set to lap(psi)
59  k, l = dist.local_modes(xbasis),dist.local_modes(ybasis)  # values of (k,l) for each sin/cos coefficient
60
61  # single vortex:
62  #vor0['g'] = vortex_vorticity(1,1,0,0,0)
63
64  # # two converging vortices:
65  # vor0['g']=vortex_vorticity(1,2,-4,0,0)+vortex_vorticity(1,-2,4,0,0)
66
67  # two indirection collision vortices:
68  vor0['g']=vortex_vorticity(1,2,-3,0,0)+vortex_vorticity(1,-2,3,6,0)
69  # # four converging vortices:
70  # vor0['g'] = vortex_vorticity(1,1,5,0,np.pi)+vortex_vorticity(1,1,0,5,-np.pi/2)+vortex_vorticity(1,1,-5,0,0)+vortex_vorticity(
71
72  # # four converging vortices with random angle
73  # vor0['g'] = vortex_vorticity(1,1,5,0,np.pi/3)+vortex_vorticity(1,1,0,5,-np.pi/6)+vortex_vorticity(1,1,-5,0,0,np.pi/8)+vortex_
74
75
76  k2l2 = -np.pi**2/4*(k**2/Lx**2+l**2/Ly**2)
77  psi['c'][k2l2!=0] = vor0['c'][k2l2!=0] /k2l2[k2l2!=0]   # divide by above factor for each coefficient to get psi from lap(psi),
78
79
80  # Analysis
81  snapshots = solver.evaluator.add_file_handler('Dipole-Vortex-Data', sim_dt=0.1, max_writes=100)
82  snapshots.add_task(psi, name='psi')
83  snapshots.add_task(d3.lap(psi), name='vorticity')
84  snapshots.add_task(d3.grad(psi)@d3.grad(psi), name='energy')
85
86  # CFL
87  CFL = d3.CFL(solver, initial_dt=max_timestep, cadence=10, safety=0.5, threshold=0.1, max_change=1.5, min_change=0.5, max_dt=max_
88  CFL.add_velocity(d3.skew(d3.grad(psi)))
89
90  # Flow properties
91  flow = d3.GlobalFlowProperty(solver, cadence=10)
92  flow.add_property(d3.integ(d3.grad(psi)@d3.grad(psi)), name='Energy')
93
94  # Main loop
95  try:
96      while solver.proceed:
97          timestep = CFL.compute_timestep()
98          solver.step(timestep)
99          if (solver.iteration-1) % 10 == 0:
100             Energy = np.sqrt(flow.max('Energy'))
101             logger.info('Iteration=%i, Time=%e, dt=%e, Energy=%f' %(solver.iteration, solver.sim_time, timestep, Energy))
102 except:
103     logger.error('Exception raised, triggering end of main loop.')
104     raise
105 finally:
106     solver.log_stats()
```

I would like to point out a few point when implementing the simulation:

5.1.1 Spectral representations of function

A spectral method discritizes functions by expanding them over a set of basis functions. Consider an orthogonal basis $\{\psi_n(x)\}$ and the spectral representation of a function $f(x)$ can be written as:

$$f(x) = \sum_{n=0}^{\infty} f_n^{\phi} \phi_n(x) \tag{31}$$

where $f_n^{\phi} = \frac{<\phi_n, f>}{<\phi_n, \phi_n>}$
Numerical spectral methods approximate function using expansions that are truncated after N nodes. The truncated coefficients $\tilde{f}_n^{\phi}$ are computed using quadrature rules of the form $\tilde{f}_n^{\phi} = \sum_{i=0}^{N-1} w_i f(x_i)$.

The error in the truncated approximation is often of the same order as the last retained coefficient. The spectral coefficients of smooth functions typically decay exponentially with n, resulting in highly accurate representations. [9]

In the code above, I have used Fourier basis where the basis can be written as following:

$$\phi_k^F(x) = exp(ikx) \tag{32}$$

and a native grid consisting of evenly spaced points: $x_i = \frac{2\pi i}{N}$ for $i = 0, \cdots, N-1$
Therefore (31) can be written as

$$f(x) = \sum_{-k_m}^{k_m} f_k \phi_k^F(x) \tag{33}$$

where $k_m = \lfloor \frac{N_c - 1}{2} \rfloor$ is the maximum resolved wave number, excluding the Nyquist node.

5.1.2 Dedalus scaling factor

Each basis has a corresponding coordinate grid that can be used for plotting fields, and the factor 'dealias=3/2' is associated with the number of points in the grid relative to the number of basis modes. The well- known "3/2 rule" states that properly dealiasing quadratic nonlinearities calculated on the grid requires a transform scale of $s \geq 3/2$, where $s = N_g/N_c$, the ratio between points in grid space and truncated modes in coefficient space.

5.1.3 Entering problem in Dedalus

The original equation we have is $\frac{\partial \nabla^2 \psi}{\partial t} = -J[\psi, \nabla^2 \psi]$. Dedalus requires the system to have everything linear on LHS and everything non-linear on the RHS.Then matrix calculation can proceed by treating the RHS as an inhomongenous term.

5.1.4 Initial condition

Since we can write ψ in 2D fourier series form as

$$\sum_{k=1}^{N} \sum_{l=1}^{N} C_{kl} \cos(\frac{k\pi x}{2L_x}) \cos(\frac{l\pi y}{2L_y}) \tag{34}$$

Then $\nabla^2 \psi$ can be written as

$$\sum_{k=1}^{N} \sum_{l=1}^{N} \frac{-\pi^2}{4} (\frac{k^2}{L_x^2} + \frac{l^2}{L_y^2}) C_{kl} \cos(\frac{k\pi x}{2L_x}) \cos(\frac{l\pi y}{2L_y}) \tag{35}$$

Then we find a relation between $\nabla^2 \psi$ and ψ in the coeficient space:

$$\psi = \frac{\nabla^2 \psi}{\frac{-\pi^2}{4}(\frac{k^2}{L_x^2} + \frac{l^2}{L_y^2})} \tag{36}$$

The reason we created an extra vorticity field is because the streamfunction is non-constant when $r > a$. As we are employing a spectral method to solve this problem, which is the underlying principle of Dedalus, we assume periodicity in the domain. Consequently, any features that vanish on the right side of the domain must smoothly reappear on the left side. Since there is zero vorticity outside the dipole vortex, no discontinuities exist in our solution.

5.1.5 Tau method

The tau term added to the equation is known as the tau method. It is extremely helpful for solving PDEs using polynomial spectral methods. Most PDEs do not have exact polynomial solutions. By adding the tau term, we can modify the original system slightly to obtain n exact polynomial solution. Chebyshev polynomials are often a convenient choice, but other types of polynomials have been used in practise.[6] An example of this is: [5]

$$\begin{cases} \frac{\partial u(x)}{\partial x} - u(x) = 0 \quad x \in [0,1] \\ u(0) = 1 \end{cases} \tag{37}$$

We know it has exact solution $u(x) = e^x$, but we want to get a polynomial solution instead. We can solve the following modified PDE:

$$\frac{\partial u(x)}{\partial x} - u(x) + \tau P(X) = 0 \tag{38}$$

with solution $u(x) = (x^2 + 2x + 2)/2$ with $\tau = 1/2$.
The tau method makes these modifications explicit in the problem rather than hiding them in the solution. The number of tau terms added to the system is the same as the number of boundary conditions we have. Additionally, the tau method also provides a conceptually straightforward way of applying gereral boundary conditions without needing a specialized basis.

5.1.6 Gauge condition

Notice we have an extra equation added into the system: $\int \psi dxdy = 0$, this is known as the Gauge condition[7]. If we add a constant term to ψ, we can still obtain the same solution. The left-hand side (LHS) of the equation can be represented as a square matrix. If we have multiple solutions and the matrix is square, then it must be degenerate. By adding the extra condition, we introduce an additional degree of freedom to the variables and a single additional constraint, making the system square and non-singular.

Here is a example: Consider solving incompressible hydrodynamics in a fully periodic domain discretized with fourier bases in each dimension.

```
problem.add_equation("div(u) = 0")
problem.add_equation("dt(u) + grad(p) - nu*lap(u) = - u@grad(u)")
```

For the mean $\vec{k} = 0$ fourier mode, the divergence equation has no spatial variation (no variation when we move along space). The divergence equation is automatically satisfied for the zero-frequency component. Since the system must solve for any RHS, which means it needs to satisfy $\nabla \cdot \vec{u} = 1$. However, it clearly doesn't satisfy this. Additional constraints or modifications are needed to ensure solvability and uniqueness of the solution.

5.1.7 Numerical viscosity

[1] In this section I would like to explain why we need to add **nu*lap(lap(psi)** into the system. Firstly consider the Jocobian term: $J[\psi, \nabla^2\psi]$. In our simulation, we uses 'Real fourier', which means both term in the Jocobian can be written as $\sum_{n=1}^{N} a_n \cos(\frac{n\pi}{L}x)$.(For simplicity, we only look at the x terms) If we calculate the Jocobian, we will obtain the following:

$$\sum_{n=1}^{N}\sum_{m=1}^{N} a_n a_m \frac{nm\pi}{L^2} \cos(\frac{n\pi}{L}x)\cos(\frac{m\pi}{L}x) \tag{39}$$

$$= \sum_{n=1}^{N}\sum_{m=1}^{N} a_n a_m \frac{nm\pi}{L^2} (\cos(\frac{(n+m)\pi}{L}x) + \cos(\frac{(n-m)\pi}{L}x)) \tag{40}$$

From (40), we realise energy in most of the mode will goes down because energy get transferred into the $n+m$ term. If we look at the $\cos\frac{N\pi}{L}x$ term: The Jocobian moves energy to the highest mode and it builds up due to the limited number of modes used in the approximation.(The energy cannot transfer into higher terms) To mitigate the aliasing and energy buildup problems, numerical viscosity is introduced as an artificial damping mechanism, **nu*lap(lap(psi))** specifically in this problem.

Since we are solving a problem using finite grid, this means everything that goes off one side appears back on the other side which will create a jump of $\frac{2a^2U}{Ly}$ known as Gibbs phenomenon[2], but this could be damped

by the numerical viscosity. The idea is similar to add more terms to the square wave (Figure 4): The width of the error continues to narrow, the area of the error – and hence the energy of the error – converges to 0. On the other hand, if we solve the problem using (28), then the jump will be $2ULy$ which could not be smooth out easily and will lead energy to tend towards infinity.

It is important to note that the choice of the viscosity coefficient (e.g., in the diffusion term nu*lap(lap(psi))) involves a trade-off between accuracy and stability.If the viscosity is set too high, it can excessively dampen the entire system.

(a) Gibbs phenomenon 50

(b) Gibbs phenomenon 250

Figure 4: Gibbs phenomenon

5.2 Single dipole vortex moving in x-axis

Firstly, let's consider the case where the vortex is moving along the x-axis. It is easy to find out the maximum of the fluid vorticity. In 2D inviscid fluid flow, we know vorticity is defined as $\nabla \times \vec{u}$, and 2D streamfunction in Cartesian coordinate is defined as

$$\begin{cases} u = \frac{\partial \psi}{\partial y} \\ v = -\frac{\partial \psi}{\partial x} \end{cases} \tag{41}$$

By combining the vorticity equation and (41), we can obtain the following: $\omega = -\nabla^2\psi$. Recall $\nabla^2\psi = -k^2\psi$, this means $\omega = k^2\psi$.
By using the fact $k = j_{1i}/a$ and (28), we obtain

$$w = \frac{2Uj_{1i}}{aJ_0(j_{1i})} J_1(\frac{j_{1i}r}{a}) \sin\theta \tag{42}$$

If we calculate the gradient of w, we obtain $r = \frac{j_{0i}a}{b} \sim 0.48a, \theta = \pm\frac{\pi}{2}$. This shows the vortex dipole has two symmetrical parts of positive and negative vorticity distributions in the lower and the upper part of the cylinder. We can calculate the circulation using a double integral:

$$\int\int \omega(r,\theta) r d\theta dr \tag{43}$$

Using mathematica Figure(5), I obtain the circulation for the upper and lower half respectively.

```
In[37]:= a = 1;
         U = 1;
         j1i = x /. FindRoot[BesselJ[1, x] == 0, {x, 3}];
         result =
          Integrate[Integrate[(2 U j1i) / (a BesselJ[0, j1i]) BesselJ[1, (j1i r) / a] Sin[θ] r,
            {θ, π, 2 π}], {r, 0, a}]
Out[40]= 6.8309

In[41]:= a = 1;
         U = 1;
         j1i = x /. FindRoot[BesselJ[1, x] == 0, {x, 3}];
         result =
          Integrate[Integrate[(2 U j1i) / (a BesselJ[0, j1i]) BesselJ[1, (j1i r) / a] Sin[θ] r,
            {θ, 0, π}], {r, 0, a}]
Out[44]= -6.8309
```

Figure 5: circulation

It shows the overall circulation is 0 since both them have same magnitude but opposite sign. Further the kinetic energy E is:

$$E = \int_0^{2\pi} \int_0^a (u^2 + v^2) r \; dr d\theta = 4\pi U^2 a^2 \tag{44}$$

5.3 Head-on collision between two dipole vortices

Figure (7) illustrates the direct collision between two vortices structures. Each vortex has a radius of $r = 1$ and is moving towards each other along the y-direction with a uniform speed of $|v| = 2$. To facilitate further analysis, let's denote the upper dipole vortices as O_1 and the lower dipole vortices as O_2. Within each dipole vortices, the left vortex is referred to as O_{i_+} and the right vortex as O_{i_-}.

As depicted in Figures (7*b*), the vortices assume a configuration known as a "quadrupole." However, this particular arrangement is inherently unstable, leading to its subsequent disintegration, as illustrated in Figure (7*c*). Since each pair of vortices, O_{1_+} & O_{2_+}; O_{1_-} & O_{2_-} undergoes opposite rotational orientations, enabling them to form a dipole structure. This is also exactly what has been shown in the diagram.

G. J. F. van Heijst & J. B. Flor (mentioned early) also vetified this result in their experiment. Although the colliding dipoles (Figure(6)) were not exactly symmetric and were slightly mis-aligned,it is clear that the dipoles exchange partners, and that two new dipoles arise, moving along straight lines away from the collision area. The reason why it is not moving along y-axis as we expected is because the mis-alignment of the original vortices.

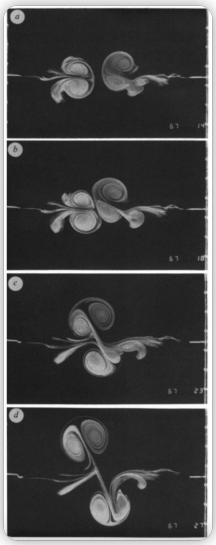

Figure 6: head-on collision experiment

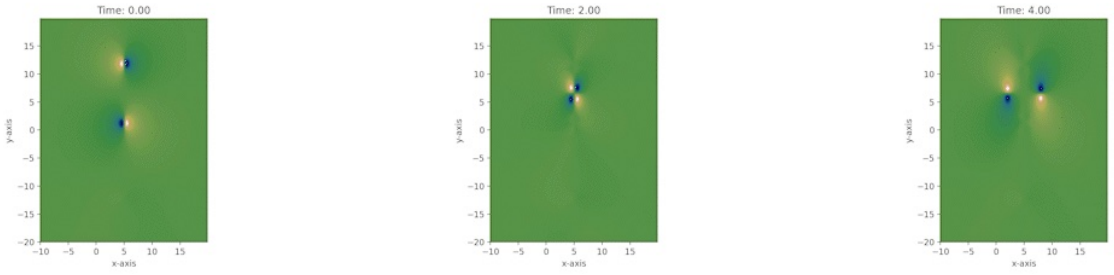

(a) two vortices direct collision 0.0 (b) two vortices direct collision 2.0 (c) two vortices direct collision 4.0

Figure 7: two vortices direct collision

5.4 Indirect collision between two vortices

Figure (8) illustrates the interaction between two vortices structures in a collision scenario. Each vortex has a radius of $r = 1$ and is moving towards each other along the y-direction with a uniform speed of $|v| = 2$. To facilitate further analysis, we denote the left lower dipole vortices as O_1 and the right upper dipole vortices as O_2. Within each dipole vortices, the left vortex is referred to as O_{i_-} and the right vortex as O_{i_+}.

Figures (8c) and (8d) describe the evolution of the dipole vortices structures as they undergo an indirect collision. Both dipole vortices undergo a slightly breakdown of their original structure. It is observed that O_{1_+} and O_{2_-} appear to become unstable and leading to the creation of thin, elongated vortex structures known as vortex filaments. A vortex filament is an imaginary spatial curve that induces a rotary flow in the space through which it passes.[10]

The formation of vortex filaments leads to a reduction in the strength of O_{1_+} and O_{2_-}, thereby disrupting the equilibrium state of the dipole vortex. As observed in Figure 8f, O_{1_-} and O_{2_+} with a higher strength induces a circular motion in the dipole vortices.

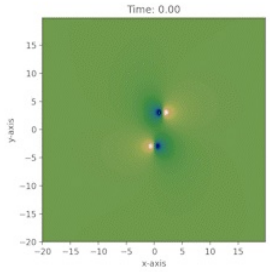

(a) two vortices indirect collision 0.0

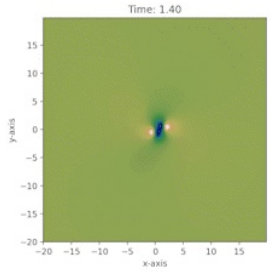

(b) two vortices indirect collision 1.4

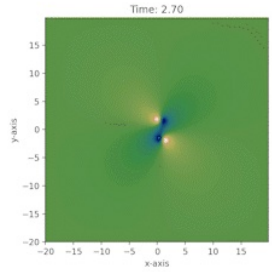

(c) two vortices indirect collision 2.7

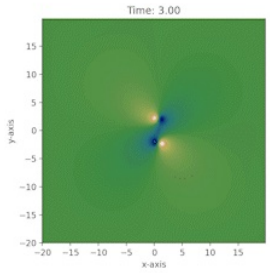

(d) two vortices indirect collision 3.0

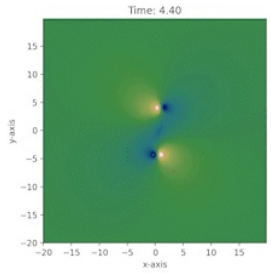

(e) two vortices indirect collision 4.4

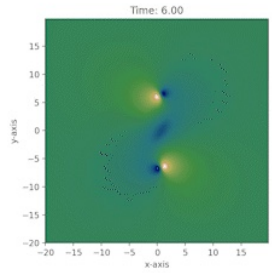

(f) two vortices indirect collision 6.0

Figure 8: two vortices indirect collision

5.5 Interaction between four vortices pair

Four dipoles are initially placed in the domain, two along the x-axis and two along the y-axis, in such a way that they move towards each other. We label the right dipole as O_1 and proceed anticlockwise with the labels O_2, O_3, and O_4, respectively. The blue vortex is always referred to as O_{i_+}, while the yellow vortex is denoted as O_{i_-}. Figure 9d illustrates that when the dipoles collide, the vortices at the diagonals are closer to the original pairs, causing the dipoles to deform. For example, O_{1_+} is closer to O_{2_-} and O_{1_-} is closer to O_{4_+}. At that moment, new dipoles are formed, which move away from the collision site. This process is very similar to the collision of two dipoles, and a vortex filament is also created during the process.

5.6 Random motion of 15 dipole vortices

In this section, I generalize the above idea further. I use the Random class to generate 15 randomly distributed dipole vortices with random velocity, orientation, and radius. During this simulation, several phenomena occur.

Firstly, in figures 10a, 10b, and 10c, we observe an indirect collision happening at position (-15, -10). The vortices experience a direct scattering, bouncing away from each other without any change in pairs occurring.

Next, when we examine figures 10d, 10e, and 10f at position (5, 15), we observe an exchange collision. The opposite dipole vortices change their pair during the collision.

Upon close inspection of the dipole vortices at the bottom-left corner (-5, -12.5), a scenario akin to a head-on collision between two dipole vortices is evident. However, a subtle alteration in motion is observed. Instead

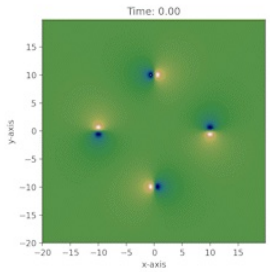

(a) four vortices collision 0.0

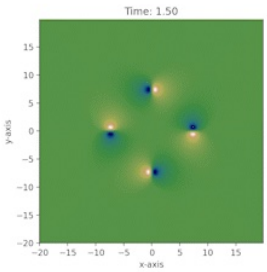

(b) four vortices collision 1.5

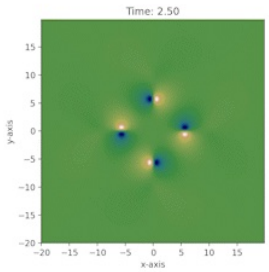

(c) four vortices collision 2.5

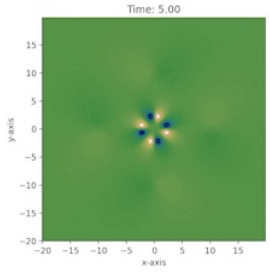

(d) four vortices collision 5

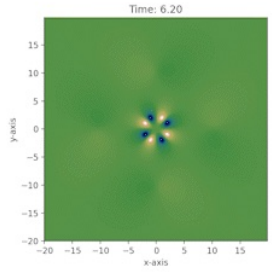

(e) four vortices collision 6.2

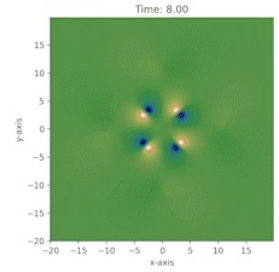

(f) four vortices collision 8.0

Figure 9: Four vortices collision

of immediately changing pairs and moving away at a 90-degree angle, the vortices with greater strength (the darker ones) retain their original trajectory. On the other hand, the vortices with lesser strength are compelled to split and eventually return to their initial states after the stronger ones have passed.

6 Point vortices model

Now we see how dipole vortices interact with other vortices numercially. Rather than studying these dipole vortices by full numerical simulation, in the paper written by 'Meleshko, V.V., and G.J.F. van Heijst' [11], they investigate the possibilities of modelling some essential features of the dynamics by a simplified model in which the dipole vortices are represented by point vortices. In this section, I will describe briefly on how they applied the point vortices model, and I will also analyse the case of two converging dipole vortices interact with each other in detail.

6.1 Formulation of point vortices model

The point vortex model is a system of N point particles of constant circulation that each generate a corresponding velocity field computed by inverting the curl operator in the vorticity–velocity relation using the Biot–Savart law.[13] The 2D problem of the interaction of N point vortices of strength κ_i and position (x_i, y_i) in the unbounded plane (x, y) of an inviscid fluid consists in solving the following equations:

$$\frac{\mathrm{d}x_i}{\mathrm{d}t} = -\frac{1}{2\pi} \sum_{j=1, j\neq i}^{N} \frac{\kappa_j y_{ij}}{l_{ij}^2} \tag{45}$$

$$\frac{\mathrm{d}y_i}{\mathrm{d}t} = \frac{1}{2\pi} \sum_{j=1, j\neq i}^{N} \frac{\kappa_j x_{ij}}{l_{ij}^2} \tag{46}$$

where $l_{ij}^2 = (x_i - x_j)^2 + (y_i - y_j)^2$ It is shown by Kirchhoff [12] that equations (45) and (46) define a Hamiltonian dynamical system:

$$\begin{cases} \kappa_i \frac{\mathrm{d}x_i}{\mathrm{d}t} = \frac{\partial H}{\partial y_i} \\ \kappa_i \frac{\mathrm{d}y_i}{\mathrm{d}t} = -\frac{\partial H}{\partial x_i} \end{cases} \tag{47}$$

with Hamiltonian H given by $H = -\frac{1}{2\pi} \sum_{i\neq j}^{N} \kappa_i \kappa_j \ln l_{ij}$
The Hamiltonian H does not depend explicitly on time and thus is a constant of the motion. Furthermore, H

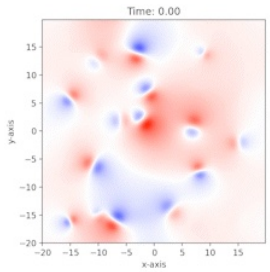

(a) Random collision model 0

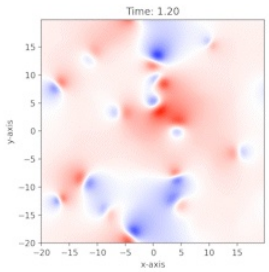

(b) Random collision model 1.2

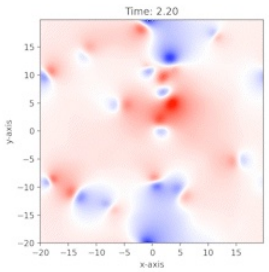

(c) Random collision model 2.2

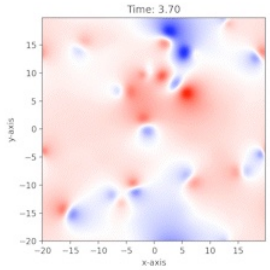

(d) Random collision model 3.7

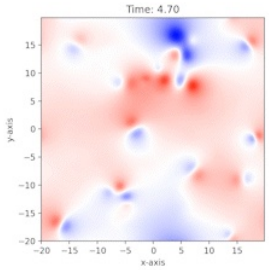

(e) Random collision model 4.7

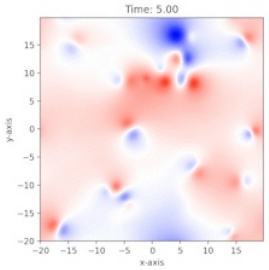

(f) Random collision model 5.0

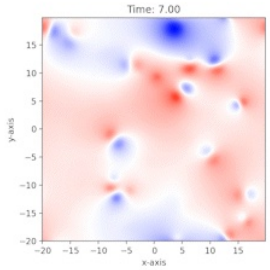

(g) Random collision model 7

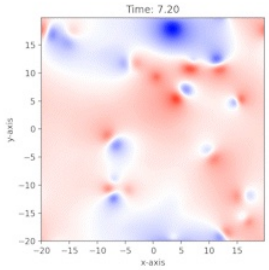

(h) Random collision model 7.2

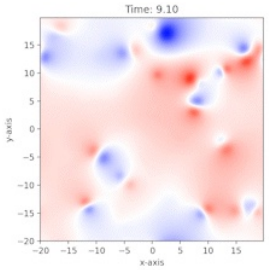

(i) Random collision model 9.1

Figure 10: Random collision model

is invariant to translation and rotation of the coordinates. These symmetries imply three conservation laws:

$$\begin{cases} Q = \sum_{i=1}^{N} \kappa_i x_i \\ P = \sum_{i=1}^{N} \kappa_i y_i \\ I = \sum_{i=1}^{N} \kappa_i (x_i^2 + y_i^2) \end{cases} \tag{48}$$

where Q,P are x,y component of conservation of the linear momentum and I is the angular momentum.

6.2 Motion of three vortices

6.2.1 Physical region

In the paper of 'Motion of three vortices' written by Aref, he described the motion of 3 vortices scattering analytically. I am going to reproduce the analytic result obtained by him in this section. Before I dive into the trajectory of the vortices, I would like to introduce the idea of physical regions.

Follows from (48) that

$$\frac{1}{2} \sum_{i,j} \kappa_i \kappa_j l_{ij}^2 = (\sum_i \kappa_i) \sum_j \kappa_j (x_j^2 + y_j^2) - (\sum_i \kappa_i x_i)^2 - (\sum_i \kappa_i y_i)^2 \tag{49}$$

is a constant of the motion which is independent of the choice of coordinates. From (45) and (46), it is possible to derive equations of motion for the vortex separations l_{ij} without reference to the absolute positions of the vortices:

$$\frac{\mathrm{d}l_{ij}^2}{\mathrm{d}t} = \frac{2}{\pi} \sum_{k \setminus i,j} \kappa_k \epsilon_{ijk} A_{ijk} (\frac{1}{l_{ij}^2} - \frac{1}{l_{ij}^2}) \tag{50}$$

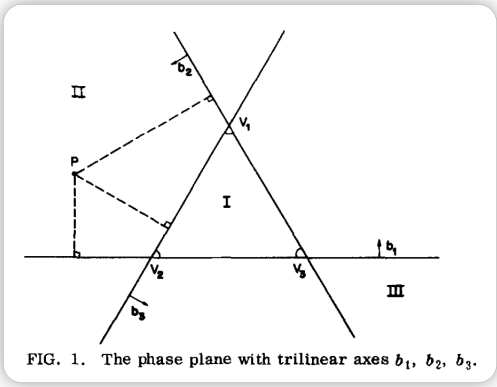

FIG. 1. The phase plane with trilinear axes b_1, b_2, b_3.

Figure 11: Aref's analyzation of three vortices collision

where A_{ijk} is the area of triangle ijk. We use the invariant (49) to define a parameter C by

$$\kappa_1\kappa_2 l_{12}^2 + \kappa_2\kappa_3 l_{23}^2 + \kappa_3\kappa_1 l_{31}^2 = 3\kappa_1\kappa_2\kappa_3 C \tag{51}$$

Then we define the dimensionless variables:

$$\begin{cases} b_1 = \frac{l_{23}^2}{\kappa_1 C} \\ b_2 = \frac{l_{31}^2}{\kappa_2 C} \\ b_3 = \frac{l_{12}^2}{\kappa_3 C} \end{cases} \tag{52}$$

such that $b_1 + b_2 + b_3 = 3$

This relation suggests introducing the b variables as trilinear coordinates in a plane, which referred to as the phase plane.

The use of this coordinate system is driven by the absence of a background flow, with the fluid motion being solely influenced by the three vortices. By employing this new coordinate system, we effectively reduce the degrees of freedom from 6 to 3, simplifying the analysis process. While the trajectory plot, presented in the subsequent section, does not provide an exact representation of the vortices' paths, it offers a convenient means to identify and classify different types of trajectories.
The triangle in figure (11) with b_i represent the distances from the sides of the triangle is in trilinear coordinates. He defined the signs of our coordinates by the arrows shown on the axes. Then that means the phase point must lie in one of the regions I,II, or III. However, only parts of these regions correspond to configurations of three vortices as the lengths l_{12}, l_{23}, l_{31} must form the sides of a triangle. In other words, it must satisfy the following equation:

$$\begin{cases} l_{12} \leq l_{23} + l_{31} \\ l_{31} \leq l_{12} + l_{23} \\ l_{23} \leq l_{31} + l_{12} \end{cases} \tag{53}$$

These valid regions is called the physical regions. We can then use (52) and (53) to find out that:

$$(k_1 b_1)^2 + (k_2 b_2)^2 + (k_3 b_3)^2 \leq 2(k_1 k_2 b_1 b_2 + k_2 k_3 b_2 b_3 + k_3 k_1 b_3 b_1) \tag{54}$$

The coefficient of (54) specify the shape of the physical region, and in here I am only interesting in one special case: $k_3 < 0, k_1 + k_2 + k_3 > 0$, the physical region will be a hyperbola. In particular, I am interested in the case when $k_1 = k_2 = -k_3 = 1$.

6.2.2 Phase Trajectories

Since within the physical region, the phase point must follow a trajectory that the Hamitionian remain constant. By substitute (52) into H, he obtained the following equation for the phase point trajectory:

$$|b_1|^{\frac{1}{k_1}} |b_2|^{\frac{1}{k_2}} |b_3|^{\frac{1}{k_3}} = \frac{1}{\theta} \tag{55}$$

where $\theta = k_1^{\frac{1}{k_1}} k_2^{\frac{1}{k_2}} k_3^{\frac{1}{k_3}} |C|^{(\frac{1}{k_1}+\frac{1}{k_2}+\frac{1}{k_3})} e^{8\pi H/(k_1 k_2 k_3)}$ Therefore the phase trajectory is given by the level curve of f:

$$f(b_1, b_2, b_3) = |b_1|^{\frac{1}{k_1}} |b_2|^{\frac{1}{k_2}} |b_3|^{\frac{1}{k_3}} \tag{56}$$

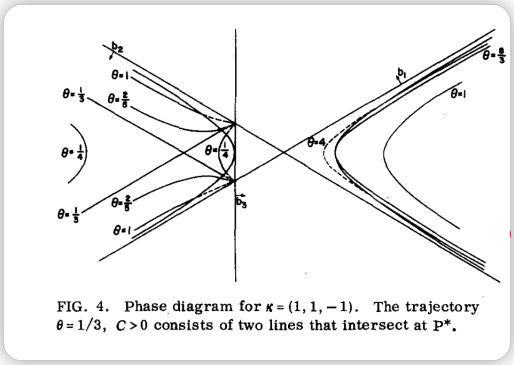

FIG. 4. Phase diagram for $\kappa = (1, 1, -1)$. The trajectory $\theta = 1/3$, $C > 0$ consists of two lines that intersect at P*.

Figure 12: Phase diagram in Aref's paper

We can find the stationary point of f, denoted P^*.

$$P^* = \frac{1}{h}(\frac{1}{k_1}, \frac{1}{k_2}, \frac{1}{k_3}) \tag{57}$$

After applying (50) to l_{12}, l_{23}, l_{31} separately, we find:

$$l_{12}^2 = l_{23}^2 = l_{31}^2 = \frac{C}{h} \tag{58}$$

The vortices form an equilateral triangle and they also doesn't change shape or size as it moves about in the fluid. When $k_3 < 0, h > 0$, P^* is a saddle point where $k_1 = k_2 = -k_3$ belong to this category.

Furthermore, if the distance between vortices b_i does not satisfy the condition described by Equation (57), the following observations can be made. Referring to the phase diagram illustrated by Aref in Figure 12, it becomes evident that the physical region is bounded by a hyperbola. Phase trajectories that diverge towards infinity indicate the scattering of a neutral pair by a single vortex. Specifically, for $C < 0$ and $0 < \theta < \frac{8}{3}$ or $C > 0$ and $0 < \theta < \frac{1}{3}$, the trajectories correspond to an exchange scattering scenario. On the other hand, when $C < 0$ and $\theta > \frac{8}{3}$ or $C > 0$ and $\theta > \frac{1}{3}$, the trajectories depict a direct scattering scenario.

6.3 Motion of four vortices system

I have modelled the simulation in Section 5.3 using the particle path model described above. It is evident that the model (Figure 13) agrees with the simulation. The vortices broke up from their original pairs, paired up with the new ones and move away in an orthornormal direction. Additionally, I have discovered that the closest distance between the vortices is 0.961, which matches the desired radius of the original vortices. Figure 13b demonstrates a significant decrease in kinetic energy at $t \approx 2$ as a result of the dipole vortices breaking apart and swapping pairs.

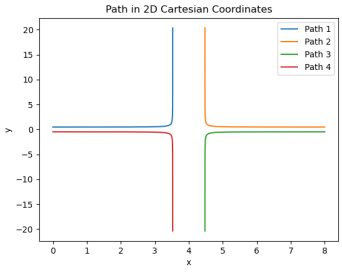

(a) four vortices collision particle path

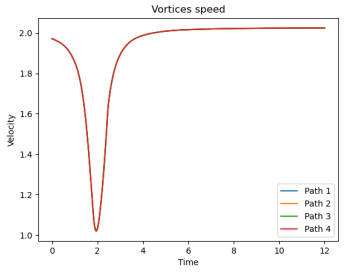

(b) four vortices collision particle speed

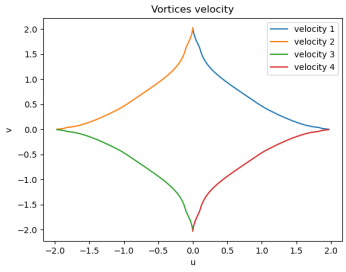

(c) four vortices collision particle velocity

Figure 13: Four vortices collision vortices model

Lydon, Karl, Sergey V Nazarenko, and Jason Laurie in their 'Dipole Dynamics in the Point Vortex Model'[13] paper uses the idea of three vortices system and derive similar result for four vortices system:

The parallelogram geometry allows them to exclude consideration of the fourth vortex from the system using the relations $l_{34} = l_{12}, l_{14} = l_{23}$, and $l_{24}^2 = 2l_{12}^2 + 2l_{23}^2 - l_{13}^2$ to arrive at a three vortex scattering problem, with a Hamiltonian

$$H = -\frac{\kappa^2}{2\pi} \frac{ln(l_{13}\sqrt{2l_{12}^2 + 2l_{23}^2 - l_{13}^2})}{l_{12}^2 l_{23}^2} \tag{59}$$

We can use the method of three vortices for this problem now. I am not going to describe them here. Detail are in 'Dipole Dynamics in the Point Vortex Model' paper.

6.4 Interaction of four vortices pairs

Not surprisingly, the results of the 8-vortex model agree with the simulation discussed in Section 5.5. The vortices break their existing pairs and form new pairs with the diagonal counterparts, resulting in diagonal movement.(Figure 14)

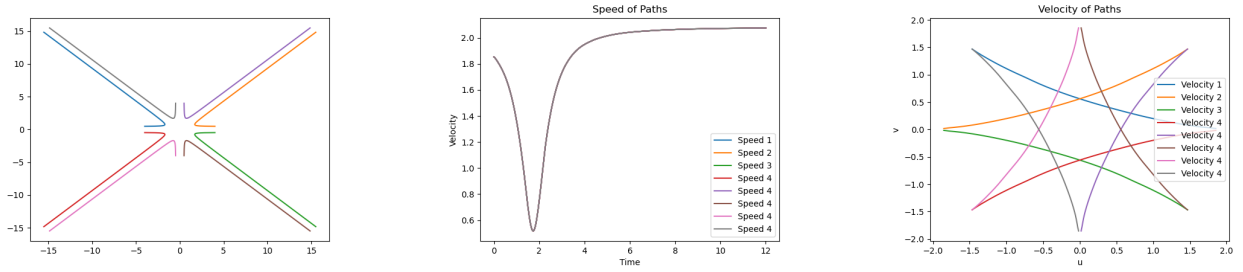

(a) four vortices pairs collision particle path

(b) four vortices pairs collision particle speed

(c) four vortices pairs collision particle velocity

Figure 14: Four vortices pairs collision vortices model

References

[1] Numerical diffusion. (n.d.). In Wikipedia. Retrieved June 17, 2023, from `https://en.wikipedia.org/wiki/Numerical_diffusion`

[2] Wikipedia contributors. Gibbs phenomenon. Wikipedia. Retrieved from `https://en.wikipedia.org/wiki/Gibbs_phenomenon#cite_note-Pinksky-4`

[3] Pedlosky, J. Geophysical Fluid Dynamics (pp. 86-94). Springer.

[4] Meleshko van Heijst 1994 (pp.166-171)

[5] The Dedalus Project. Tau Method. Dedalus Project Documentation. Retrieved from `https://dedalus-project.readthedocs.io/en/latest/pages/tau_method.html`

[6] Numerical solution of nonlinear partial differential equations with the Tau method, Journal of Computational and Applied Mathematics (1985) 511-516. by E.L. ORTIZ and K.-S. PUN

[7] The Dedalus Project. Gauge condition. Dedalus Project Documentation. Retrieved from `https://dedalus-project.readthedocs.io/en/latest/pages/gauge_conditions.html`

[8] van Heijst, G. J. F, and J. B Flór. "Dipole Formation and Collisions in a Stratified Fluid." Nature (London) 340.6230 (1989): 212–215. Web.

[9] PhysRevResearch.2.023068, Dedalus: A flexible framework for numerical simulations with spectral methods. Burns, Keaton J. and Vasil, Geoffrey M. and Oishi, Jeffrey S. and Lecoanet, Daniel and Brown, Benjamin P. 2020 Apr. Page 2

[10] Snorri Gudmundsson, Chapter 9 - The Anatomy of the Wing, Editor(s): Snorri Gudmundsson, General Aviation Aircraft Design, Butterworth-Heinemann, 2014, Pages 299-399, ISBN 9780123973085

[11] Meleshko, V.V., and G.J.F. van Heijst. "Interacting Two-Dimensional Vortex Structures: Point Vortices, Contour Kinematics and Stirring Properties." Chaos, solitons and fractals 4.6 (1994): 977–1010. Web.

[12] G. Kirchhoff, Vorlesungen iiber Mathematische Physik. Mechanik. Teubner, Leipzig (1876).

[13] Lydon, Karl, Sergey V Nazarenko, and Jason Laurie. “Dipole Dynamics in the Point Vortex Model.” Journal of physics. A, Mathematical and theoretical 55.38 (2022): 385702–. Web.

[14] Aref, Hassan. “Motion of Three Vortices.” The Physics of fluids (1958) 22.3 (1979): 393–400. Web.